

Amplitude equations and pattern selection in Faraday waves

By PEILONG CHEN¹ AND JORGE VIÑALS^{1,2}

¹Supercomputer Computations Research Institute, Florida State University, Tallahassee,
Florida 32306-4130, USA

² Department of Chemical Engineering, FAMU-FSU College of Engineering, Tallahassee,
Florida 31310-6046, USA

(Received 1 November 2018)

A nonlinear theory of pattern selection in parametric surface waves (Faraday waves) is presented that is not restricted to small viscous dissipation. By using a multiple scale asymptotic expansion near threshold, a standing wave amplitude equation is derived from the governing equations. The amplitude equation is of gradient form, and the coefficients of the associated Lyapunov function are computed for regular patterns of various symmetries as a function of a viscous damping parameter γ . For $\gamma \sim 1$, the selected wave pattern comprises a single standing wave (stripe pattern). For $\gamma \ll 1$, patterns of square symmetry are obtained in the capillary regime (large frequencies). At lower frequencies (the mixed gravity-capillary regime), a sequence of six-fold (hexagonal), eight-fold, . . . patterns are predicted. For even lower frequencies (gravity waves) a stripe pattern is again selected. Our predictions of the stability regions of the various patterns are in quantitative agreement with recent experiments conducted in large aspect ratio systems.

1. Introduction

This paper extends an earlier calculation by Zhang & Viñals (1997) of the amplitude equation governing Faraday waves in the weakly nonlinear regime. In order to make the problem analytically tractable, they neglected without rigorous justification viscous terms in the boundary conditions at the free fluid surface that had a nonlinear dependence on either the surface displacement away from planarity, or on the surface velocity. Even though the resulting amplitude equation led to the prediction of stationary patterns that are generally in agreement with experiments conducted in the regime of weak viscous dissipation (Kudrolli & Gollub (1996), Binks & van de Water (1997)), the unsystematic nature of the truncation makes it difficult to assess the range of validity of the theory. In particular, the so-called stripe pattern (a pattern comprised of a single standing wave) which is generically observed when viscous dissipation is not small, could not be obtained in their analysis for any range of parameters. We extend below this earlier work, and present a systematic weakly nonlinear theory of Faraday waves. Our results on pattern selection agree with those of Zhang & Viñals (1996) and (1997) in the limit of small viscous dissipation, and with recent experimental work otherwise.

Parametrically driven surface waves (also known as Faraday waves) can be excited on the free surface of a fluid layer that is periodically vibrated in the direction normal to the surface at rest when the amplitude of the driving acceleration is large enough to overcome the dissipative effect of fluid viscosity (Faraday (1831), Miles & Henderson (1990)). Of

special concern to us is the issue of pattern selection in a layer of lateral dimension much larger than the excited wavelength (see, e.g., Cross & Hohenberg (1993) for a recent review on pattern formation). In the case of Faraday waves, it is now known that different wave patterns can be excited depending on the fluid properties and the driving amplitude or frequency. At high viscous dissipation (a fluid of large viscosity and/or a low driving frequency), the observed wave pattern above threshold consists of parallel stripes (Edwards & Fauve (1994) and Daudet et al. (1995)). For lower dissipation, patterns of square symmetry (combinations of two perpendicular plane waves) are observed in the capillary regime (large frequencies) (Lang (1962), Ezerskii, Rabinovich, Reutov & Starobinets (1986), Tuffiaro, Ramshankar & Gollub (1989), Ciliberto, Douday & Fauve (1991) Christiansen, Alstrøm & Levinsen (1992), Müller (1993), Edwards & Fauve (1994)). At lower frequencies (the mixed gravity-capillary regime), higher symmetry patterns have been observed by Kudrolli & Gollub (1996) (hexagonal) and Binks & van de Water (1997) (hexagonal, eight- and ten-fold). The aim of this paper is to present a weakly nonlinear analysis of Faraday waves that predicts stationary wave patterns with these symmetries.

The derivation of an amplitude equation is a classical method to describe excited states beyond linear instability. Just above threshold, the evolution of the system is assumed to be described in terms of the complex amplitude A of the most unstable mode according to linear theory. The equation of motion for A is often of the form

$$\frac{dA}{dt} = \alpha A - gA^3, \quad (1.1)$$

where α is the linear growth rate, and $g > 0$ is real. The low order nonlinear term provides saturation. There exist cases, however, in which spatial isotropy permits waves to be excited in any direction, and the nonlinear interaction term in the equation above contains terms of the form $g_{ij}|A_j|^2 A_i$, with A_i and A_j the slowly varying amplitudes of two degenerate unstable modes. If the coupling coefficients g_{ij} are known, the resulting wave pattern can be predicted from Eq. (1.1), as has been illustrated by Müller (1994) for Faraday waves.

The derivation of amplitude equations for surface waves is greatly simplified in the case of an ideal (inviscid) fluid. Since the bulk flow is irrotational, there exists a hamiltonian formulation in which the canonically conjugate variables are the surface displacement and the velocity potential at the free surface (Zakharov (1968), Miles (1977)). As a consequence, early analyses of Faraday waves were based on the hamiltonian description of the inviscid limit, and treated viscous or dissipative effects as a perturbation (Miles (1984), Milner (1991), Miles (1993)). The derivation usually starts from the set of ideal fluid equations (Benjamin & Ursell (1954)), written in terms of the surface velocity potential ϕ . The linear or zero-th order solution ϕ_0 is a sum over waves of frequency ω and wavevector $\{\mathbf{k}_j\}$, with ω and $k = \|\mathbf{k}_j\|$ related by the ideal fluid dispersion relation (Eq. (2.13) below):

$$\phi_0 = \frac{-i\omega}{k} e^{kz} \sum_j A_j(T) e^{i(\mathbf{k}_j \cdot \mathbf{x} - \omega t)} + c.c.,$$

where $T = \epsilon t$ is a slow time scale, with $\epsilon \ll 1$ the dimensionless distance away from threshold. An expansion of the ideal fluid equations to third order in ϵ yields the equation for $A_j(T)$ (Milner (1991))

$$\frac{dA_j}{dT} = -\frac{ikf}{4\omega} A_{-j}^* + i \sum_k \Pi_{jk}^{(1)} |A_k|^2 A_j + i \sum_k \Pi_{jk}^{(2)} A_k A_{-k} A_{-j}^*, \quad (1.2)$$

with f the amplitude of the driving acceleration, and Π *real* functions of the angle between

the j -th and k -th wavevectors. Since the coefficients of the cubic terms are imaginary, these terms do not contribute to wave saturation. This can be seen, for example, by computing $d|A_j|^2/dT$ and observing that all cubic terms cancel. This is also a manifestation of a general symmetry principle in hamiltonian (or reversible) systems that prohibits *real* coefficients of cubic nonlinear terms in standing wave amplitude equations (Cross & Hohenberg (1993), Couillet, Frisch & Sonino (1994)).

In the limit of low viscous dissipation, Hamilton's equations have been supplemented with a dissipation function (Miles (1984), Milner (1991), Miles (1993)), which is computed under the assumption that the dominant contribution to viscous dissipation arises from the irrotational velocity field in the bulk, and not from friction at the container walls or dissipation near the free surface (where vorticity is produced). Under this assumption, the rate of energy loss is given by (Landau & Lifshitz (1959)),

$$\dot{E} = -2\eta \int dV \left(\frac{\partial^2 \phi}{\partial x_i \partial x_j} \right)^2,$$

where η is the shear viscosity, and the integral extends over the bulk fluid. The velocity potential ϕ is now expanded in powers of ϵ , and viscous contributions computed order by order in ϵ . This procedure leads to imaginary components in the coefficients of the cubic terms of Eq. (1.2), and therefore to wave saturation. The precise functional form of the coefficients obtained by this method is still somewhat controversial (Miles (1993), Hansen & Alstrøm).

We next address the effect of the rotational component of the flow. The dimensionless group involving the ratio of viscous to inertial effects is the damping parameter $\gamma = 2\nu k_0^2/\omega_0$, where k_0 is the critical wavenumber in the inviscid limit, and ω_0 its angular frequency (γ is inversely proportional to the Reynolds number of the flow). Lundgren & Mansour (1988) considered an expansion of the governing equations and boundary conditions in powers of γ . They showed that in the weak dissipation limit, the dominant terms in the boundary conditions are $\mathcal{O}(\gamma)$, with a first correction at $\mathcal{O}(\gamma^{3/2})$. At *linear* order in the surface displacement or surface velocity, terms of $\mathcal{O}(\gamma)$ are purely irrotational, while the rotational flow component contributes at $\mathcal{O}(\gamma^{3/2})$. In fact, linear stability analysis of Faraday waves by Müller *et al.* (1997) (see also Sec. 2) shows that the dimensionless value of the driving amplitude at threshold equals γ , with a first correction term that is proportional to $\gamma^{3/2}$. The dominant contribution arises solely from the irrotational flow component, with contributions from the rotational component coming at $\mathcal{O}(\gamma^{3/2})$. However, Zhang & Viñals (1997) argued that the lowest order contribution from both irrotational and rotational components is $\mathcal{O}(\gamma)$ at the nonlinear level in the surface variables. Hence rotational flow cannot be neglected in a nonlinear theory, even in the limit of small dissipation. For example, the kinematic boundary condition at the free surface does include one such term proportional to γ that arises from the component normal to the surface of the rotational part of the velocity field. This term was retained both in the analysis of Zhang & Viñals (1997) and in our analysis below, but not in previous approaches based on a dissipation function.

Another qualitative feature of importance to pattern selection in Faraday waves is triad resonant interactions. Since the standing wave amplitude equation must be invariant under $A_j \rightarrow -A_j$, † triad resonance cannot contribute directly to quadratic order in

† The governing equations are invariant under time translation by a period of the driving force $t \rightarrow T + 2\pi/\omega$. Subharmonic response implies that $\zeta(x, y, t + 2\pi/\omega) = -\zeta(x, y, t)$, with $z = \zeta(x, y, t)$ the position of the surface. Because of this invariance, the amplitude equation for A_j must also be invariant under a sign change in A_j

A_j , but it does contribute significantly to the coefficients of the cubic order term via the coupling of the zero-th order unstable wave and first order stable waves. This resonance was already encountered by Milner (1991) as a divergence of the cubic coefficient in the standing wave amplitude equation at a particular angle. Later, Edwards & Fauve (1994) suggested that triad resonance would be important at low viscous dissipation, range in which linearly stable modes are only weakly damped. Zhang & Viñals (1997) calculated such a contribution explicitly, and showed that it is important in determining the symmetry of the selected pattern in the region of small γ . In particular, they predicted a sequence of quasi-periodic patterns in the region in which the resonant angle approaches zero.

We extend in this paper the analysis of Zhang & Viñals (1997) that was based on a quasi-potential approximation to the governing equations. By separating the rotational flow within a small vortical layer near the free surface from the potential flow in the bulk, they derived a standing wave amplitude equation valid in the limit of small viscous dissipation. The calculation, however, relied on an uncontrolled approximation concerning nonlinear viscous terms and, as a consequence, its region of validity is difficult to assess. We describe below a systematic expansion of the Navier-Stokes equation and boundary conditions that overcomes this difficulty and that leads to an amplitude equation not restricted to small viscous dissipation. We start by deriving an exact, although implicit, relation for the threshold of instability, which is then used in the nonlinear analysis. This result extends earlier numerical work by Kumar & Tuckerman (1994), and agrees with a recent low viscosity approximation to the governing equations by Müller *et al.* (1997). We then use a multiple scale expansion to derive a standing wave equation which is of gradient form. Minimization of the associated Lyapunov function leads to the prediction of stationary patterns of different symmetries as a function of the fluid parameters and frequency of the driving acceleration. Our predictions are in good agreement with experiments conducted in large aspect ratio cells.

2. Governing equations and linear stability

We consider a semi-infinite fluid layer, unbounded in the $x - y$ direction, extending to $z = -\infty$, and with a planar free surface at $z = 0$ when at rest. The fluid is assumed incompressible and Newtonian. Under periodic vibration of the layer in the direction normal to the surface at rest, the equation governing fluid motion (in the co-moving reference frame) is

$$\partial_t \mathbf{u} + (\mathbf{u} \cdot \nabla) \mathbf{u} = -\frac{1}{\rho} \nabla p + \nu \nabla^2 \mathbf{u} + g_z(t) \hat{\mathbf{e}}_z, \quad (2.1)$$

with \mathbf{u} the velocity field, p the pressure, ρ and ν the density and kinematic viscosity of the fluid respectively, and $g_z(t) = -g - f \cos \omega t$ the effective gravity. † The base state is a quiescent fluid with a pressure distribution $p = \rho g_z(t) z$. We absorb the body force in the pressure, so that in what follows p is the deviation from $\rho g_z(t) z$. By applying $-(\nabla \times \nabla \times)$ to Eq. (2.1), one can eliminate the pressure term, and also obtain a system of equations for the velocity components of $\mathbf{u} = (u, v, w)$, in which the linear terms are uncoupled,

$$\partial_t \nabla^2 \mathbf{u} - \nu \nabla^2 \nabla^2 \mathbf{u} = \nabla \times \nabla \times (\mathbf{u} \cdot \nabla) \mathbf{u}. \quad (2.2)$$

† We use a driving acceleration proportional to $\cos \omega t$ instead of $\sin \omega t$ as in Zhang & Viñals (1997) to avoid, as discussed in that reference, the complication related to the parity under time reversal of the driving acceleration.

Continuity, $\nabla \cdot \mathbf{u} = 0$, has also been used to derive Eq. (2.2).

Besides the null conditions at $z = -\infty$, there are four boundary conditions at the moving free surface (Lamb (1945)). Let $z = \zeta(x, y)$ be the position of the surface (Fig. 1), then the outward pointing unit normal $\hat{\mathbf{n}}$ is

$$\hat{\mathbf{n}} = \frac{(-\partial_x \zeta, -\partial_y \zeta, 1)}{[1 + (\partial_x \zeta)^2 + (\partial_y \zeta)^2]^{1/2}}. \quad (2.3)$$

Two linearly independent tangential unit vectors $\hat{\mathbf{t}}_1$ and $\hat{\mathbf{t}}_2$ are

$$\hat{\mathbf{t}}_1 = \frac{(1, 0, \partial_x \zeta)}{[1 + (\partial_x \zeta)^2]^{1/2}}, \quad \hat{\mathbf{t}}_2 = \frac{(0, 1, \partial_y \zeta)}{[1 + (\partial_y \zeta)^2]^{1/2}}. \quad (2.4)$$

Note that these two vectors are not mutually orthogonal. The choice is made so that the expressions for $\hat{\mathbf{t}}_1$ and $\hat{\mathbf{t}}_2$ are symmetric in the Cartesian variables x and y .

The kinematic boundary condition is,

$$\partial_t \zeta + (\mathbf{u}(z = \zeta) \cdot \nabla_H) \zeta = w(z = \zeta),$$

with $\nabla_H = \hat{\mathbf{e}}_x \partial_x + \hat{\mathbf{e}}_y \partial_y$. Since the governing equations will be expanded and solved order by order, we quote here its Taylor expansion around $z = 0$,

$$\partial_t \zeta + [u + \partial_z u \zeta]_{z=0} \partial_x \zeta + [v + \partial_z v \zeta]_{z=0} \partial_y \zeta = [w + \partial_z w \zeta + \frac{1}{2} \partial_{zz} w \zeta^2]_{z=0}. \quad (2.5)$$

Only terms up to third order in the velocity or surface displacement will be required. †

Neglecting the effect of the air phase above the fluid, the tangential stress at the free surface is zero,

$$\hat{\mathbf{t}}_m \cdot \mathbf{T} \cdot \hat{\mathbf{n}}|_{z=\zeta} = 0, \quad m = 1, 2,$$

with \mathbf{T} the stress tensor of components, $T_{ij} = [-p - \rho g_z(t)z] \delta_{ij} + \rho \nu (\partial_j u_i + \partial_i u_j)$. The normal stress at the fluid surface is balanced by capillarity,

$$\hat{\mathbf{n}} \cdot \mathbf{T} \cdot \hat{\mathbf{n}}|_{z=\zeta} = 2H\sigma,$$

where σ is the surface tension and $2H$ is the mean curvature of the surface,

$$2H = \{ \partial_{xx} \zeta [1 + (\partial_y \zeta)^2] + \partial_{yy} \zeta [1 + (\partial_x \zeta)^2] - 2\partial_x \zeta \partial_y \zeta \partial_{xy} \zeta \} / [1 + (\partial_x \zeta)^2 + (\partial_y \zeta)^2]^{3/2}.$$

The linear stability of the fluid layer under vibration was first addressed in the inviscid limit by Benjamin & Ursell (1954), and later by Landau & Lifshitz (1976) in the limit of low viscosity. More recently, Kumar & Tuckerman (1994) numerically computed the neutral stability curve for a fluid of arbitrary viscosity, and Müller *et al.* (1997) have given an analytic low viscosity expansion. We first review briefly the formulation of Kumar & Tuckerman (1994), and then show that an exact (albeit implicit) analytical expression for the threshold can be derived, thus avoiding the numerical calculation.

The dominant response of the parametrically driven system is subharmonic at a frequency $\omega/2$ (Benjamin & Ursell (1954)). Although the methodology discussed below can also be used to analyze a possible harmonic response, we restrict our analysis to the subharmonic case. To address the linear stability of the fluid surface, we consider the following solutions for the vertical velocity field and surface displacement,

$$w_0 = \cos(kx) \sum_{j=1,3,5,\dots} e^{ji\omega t/2} w_0^j(z) A_j + \text{c.c.} \quad (2.6)$$

† In order to avoid excessive use of parentheses, we follow the convention in the remainder of the paper that the operator ∂ acts only on the function immediately following it.

$$\zeta_0 = \cos(kx) \sum_{j=1,3,5,\dots} e^{ji\omega t/2} A_j + \text{c.c.}$$

where the A_j are complex amplitudes, and we retain all the harmonics of the fundamental mode $e^{i\omega t/2}$. Truncation of the sums to include the fundamental mode $e^{i\omega t/2}$ alone is only appropriate for small viscous damping. From Eq. (2.2), the linearized equation of motion for w_0 is

$$(\partial_t \nabla^2 - \nu \nabla^2 \nabla^2) w_0 = 0.$$

Substituting w_0 and ζ_0 from (2.6), one finds

$$\left[\frac{1}{2} j i \omega (-k^2 + \partial_{zz}) - \nu (-k^2 + \partial_{zz})^2 \right] w_0^j(z) = 0.$$

The solution of this equation is a linear combination of $e^{\pm kz}$ and $e^{\pm q_j z}$, with $q_j^2 = k^2 + j i \omega / 2\nu$. The linearized kinematic and tangential stress boundary conditions are

$$\begin{aligned} \partial_t \zeta_0 - w_0 &= 0, \\ (\nabla_H^2 - \partial_{zz}) w_0 &= 0. \end{aligned} \quad (2.7)$$

By using the boundary conditions (2.7) and the null conditions at $z = -\infty$, $w_0^j(z)$ is given by

$$w_0^j(z) = \left(\frac{1}{2} j i \omega + 2\nu k^2 \right) e^{kz} - 2\nu k^2 e^{q_j z}.$$

The first term on the right hand side is the irrotational component of the flow, in which we have explicitly separated the inviscid and viscous contributions. The second term in the right hand side is the rotational component (this is the component that has been neglected in earlier work by Milner (1991) and Miles (1993)). The linearized normal stress boundary condition is, after having eliminated the pressure by using the equation of motion,

$$[2\nu \nabla_H^2 - (\partial_t - \nu \nabla^2)] \partial_z w_0 + \left(g - \frac{\sigma}{\rho} \nabla_H^2 + f \cos \omega t \right) \nabla_H^2 \zeta_0 = 0. \quad (2.8)$$

By substituting the assumed solutions given by Eqs. (2.6) into this equation, we note that the term $2\nu \nabla_H^2 \partial_z w_0$ when acting on the irrotational flow component e^{kz} yields a contribution at low viscosity that scales as ν , whereas the rotational contribution (from $e^{q_j z}$) scales as $\nu^{3/2}$. The remaining term $(\partial_t - \nu \nabla^2) \partial_z w_0$ is simply equal to $-\omega^2$. Hence it is justified to neglect the rotational flow component in the linear stability analysis at low damping. As we show below, and in agreement with the work by Müller *et al.* (1997), rotational flow contributes terms of order $\nu^{3/2}$ and higher to the value of the driving acceleration at onset. In the analysis that follows, however, we will retain the full linear solution.

By equating the coefficients of each harmonic $e^{ji\omega t/2}$ resulting from Eq. (2.8), Kumar & Tuckerman (1994) found

$$\begin{aligned} H_1 A_1 - f A_1^* - f A_3 &= 0, \\ H_3 A_3 - f A_1 - f A_5 &= 0, \\ H_5 A_5 - f A_3 - f A_7 &= 0, \dots \end{aligned} \quad (2.9)$$

with

$$H_j = 2 \left\{ \nu^2 [4q_j k^4 - k(q_j^2 + k^2)^2] - g k^2 - \frac{\sigma}{\rho} k^4 \right\} / k^2.$$

This is a system of equations in the unknowns A_j , function of wavenumber k and driving amplitude f . By truncating the system (2.9) at some particular A_n , it can be solved

numerically as an eigenvalue problem, f being the eigenvalue. This is indeed what was done by Kumar & Tuckerman (1994). However we observe that after truncation at A_n ,

$$A_n = \frac{f A_{n-2}}{H_n}, \quad A_{n-2} = \frac{f A_{n-4}}{H_{n-2} - \frac{f^2}{H_n}}, \quad \dots \quad (2.10)$$

so that the infinite set of equations can be re-written as

$$\left(H_1 - \frac{f^2}{H_3 - \frac{f^2}{H_5 - \dots}} \right) A_1 - f A_1^* \equiv \bar{H}_1(k, f) A_1 - f A_1^* = 0. \quad (2.11)$$

For a given wavenumber k , its threshold of instability f_k is given implicitly by

$$f_k = |\bar{H}_1(k, f_k)| = \left| H_1 - \frac{f_k^2}{H_3 - \dots} \right|. \quad (2.12)$$

The complex amplitude A_j can then be recursively obtained from Eq. (2.10) and (2.11) up to a real factor. The critical wavenumber for instability k_{onset} corresponds to the lowest value of f_k , f_0 .

It is interesting to consider the limiting behavior of Eq. (2.12) at low viscosity. First recall that for a semi-infinite inviscid fluid, the dispersion relation for surface waves is (Landau & Lifshitz (1959))

$$\omega_0^2 = g k_0 + \sigma k_0^3 / \rho, \quad (2.13)$$

with $\omega_0 = \omega/2$, and k_0 the wavenumber. In a fluid of low viscosity we expect k_{onset} to be near k_0 . It is then convenient to define dimensionless variables by using $1/\omega_0$ as the time scale, and $1/k_0$ as the length scale. We also define a reduced wave number $\bar{k} = k/k_0$, a viscous damping coefficient $\gamma = 2\nu k_0^2/\omega_0$, the gravity wave $G = g k_0/\omega_0^2$ and capillary wave $\Sigma = \sigma k_0^3/\rho\omega_0^2$ contributions to the dispersion relation, and the dimensionless amplitude of the driving acceleration $\Delta = f k_0/4\omega_0^2$. Note that $G + \Sigma = 1$ from Eq. (2.13); $G = 1$ corresponds to a pure gravity wave while $G = 0$ to a pure capillary wave. For $\gamma \ll 1$, k_{onset} and Δ_{onset} in Eq. (2.12) can be expanded as a power series of the damping coefficient γ

$$\begin{aligned} \bar{k}_{\text{onset}} &= 1 + \frac{1}{3-2G}\gamma^{3/2} + \frac{-7+2G}{(3-2G)^2}\gamma^2 + \dots, \\ \Delta_{\text{onset}} &= \gamma - \frac{1}{2}\gamma^{3/2} + \frac{11-2G}{8(3-2G)}\gamma^{5/2} + \dots \end{aligned} \quad (2.14)$$

The first correction term is proportional to $\gamma^{3/2}$, and agrees with a low viscosity expansion of the linearized equations given by Müller *et al.* (1997). As an example, we plot in Fig. 2 the value of the threshold, Δ_{onset} , as a function of γ at $G = 1/3$. Previous low damping calculations of the standing wave amplitude equation by Milner (1991), Miles (1993) and Zhang & Viñals (1997) considered the dominant term $\Delta_{\text{onset}} = \gamma$ only. Note, however, that the first correction, $-\frac{1}{2}\gamma^{3/2}$, can be a sizable contribution even for small γ (e.g., a 15% difference at $\gamma = 0.1$). As a reference, we note that a similar linear analysis based on an inviscid formulation to which viscosity is added through a dissipation function, leads to the the damped Mathieu equation,

$$\partial_t^2 \hat{\zeta}_k(t) + \gamma \partial_t \hat{\zeta}_k(t) + \omega_0^2 (1 + 2\Delta \cos 2\omega_0 t) \hat{\zeta}_k(t) = 0,$$

where $\hat{\zeta}_k(t)$ is the Fourier transform of $\zeta(x, t)$. This equation gives a threshold at $\gamma + 3\gamma^2/64 + O(\gamma^3)$, which is plotted as the dot-dashed line in Fig. 2. The first correction term is of a different order and has a different sign. Finally, we mention that rotational flow at the linear level in the surface variables can be incorporated into the damped Mathieu equation, as shown by Nam Hong (1993).

3. Standing wave amplitude Equation

In this section, we use the multiple scale approach of Newell & Whitehead (1969) to derive standing wave amplitude equations valid near threshold. It is interesting to note that the solvability condition in this case arises from the boundary conditions, unlike most other problems. For a driving amplitude f above threshold, we define $\epsilon = (f - f_0)/f_0$ and expand the flow as

$$\mathbf{u} = \epsilon^{1/2} \mathbf{u}_0 + \epsilon \mathbf{u}_1 + \epsilon^{3/2} \mathbf{u}_2 + \dots,$$

and similarly for p and ζ . Near threshold, i.e., for $\epsilon \ll 1$, we separate fast and slow time scales: $T = \epsilon t$; $\partial_t \rightarrow \partial_t + \epsilon \partial_T$. Spatial slow scales are not included because only regular patterns are considered here. At order $\epsilon^{1/2}$ we recover the linear problem discussed in the previous section. Since we are interested in standing wave patterns of different symmetries, the solution at this order is written as a linear combination of waves with wavevectors \mathbf{k}_m of magnitude k_{onset} but along different directions on the x - y plane,

$$\begin{aligned} w_0 &= \sum_m \cos(\mathbf{k}_m \cdot \mathbf{x}) B_m(T) \sum_{j=1,3,5,\dots} e^{ji\omega t/2} w_0^j(z) e_j + \text{c.c.} \\ \zeta_0 &= \sum_m \cos(\mathbf{k}_m \cdot \mathbf{x}) B_m(T) \sum_{j=1,3,5,\dots} e^{ji\omega t/2} e_j + \text{c.c.}, \end{aligned}$$

where $B_m(T)$ are *real* wave amplitudes, functions only of the slow time scale T , and the e_j are the same as the A_j found in Eqs. (2.10) and (2.11).

At order ϵ the equation of motion is

$$(\partial_t \nabla^2 - \nu \nabla^2 \nabla^2) w_1 = [\nabla \times \nabla \times (\mathbf{u}_0 \cdot \nabla) \mathbf{u}_0] \cdot \hat{\mathbf{e}}_z. \quad (3.1)$$

By using the linear solution, the right hand side of Eq. (3.1) is of the form,

$$\sum_{mn}' \cos((\mathbf{k}_m \pm \mathbf{k}_n) \cdot \mathbf{x}) \sum_{j=0,1,2,\dots} e^{ji\omega t} h_j(z). \quad (3.2)$$

The first summation is over all possible $\mathbf{k}_m \pm \mathbf{k}_n$, except zero, and the $h_j(z)$ are combinations of exponential functions. Since every term in the right hand side contains a periodic function of \mathbf{x} , and exponential functions of t and z , the particular solution of Eq. (3.1), w_{1p} , can be easily found. The homogeneous solution w_{1h} and ζ_1

$$\begin{aligned} w_{1h} &= \sum_{mn}' \cos((\mathbf{k}_m \pm \mathbf{k}_n) \cdot \mathbf{x}) \left[\sum_{j=1,2,3,\dots} e^{ji\omega t} \left(e^{|\mathbf{k}_m \pm \mathbf{k}_n|z} \alpha_{mn}^{j\pm} + e^{r_{mn}^{\pm} z} \beta_{mn}^{j\pm} \right) + \text{c.c.} \right. \\ &\quad \left. + e^{|\mathbf{k}_m \pm \mathbf{k}_n|z} \alpha_{mn}^{0\pm} + z e^{|\mathbf{k}_m \pm \mathbf{k}_n|z} \beta_{mn}^{0\pm} \right]. \\ \zeta_1 &= \sum_{mn}' \cos((\mathbf{k}_m \pm \mathbf{k}_n) \cdot \mathbf{x}) \left[\sum_{j=1,2,3,\dots} e^{ji\omega t} \delta_{mn}^{j\pm} + \text{c.c.} + \delta_{mn}^{0\pm} \right], \end{aligned} \quad (3.3)$$

must now satisfy the boundary conditions. We have defined $(r_{mn}^{\pm})^2 = |\mathbf{k}_m \pm \mathbf{k}_n|^2 + ji\omega/\nu$. The constants α_{mn} , β_{mn} and δ_{mn} are determined by the boundary conditions. At this order the boundary conditions are,

$$\begin{aligned} \partial_t \zeta_1 - w_1 &= G_{11}(\mathbf{u}_0, \zeta_0) \\ (\nabla_H^2 - \partial_{zz}) w_1 &= G_{12}(\mathbf{u}_0, \zeta_0) \\ (-\partial_t + 3\nu \nabla_H^2 + \nu \partial_{zz}) \partial_z w_1 + (g - \frac{\sigma}{\rho} \nabla_H^2 + f_0 \cos \omega t) \nabla_H^2 \zeta_1 &= G_{13}(\mathbf{u}_0, \zeta_0). \end{aligned}$$

where the functions G_{11} , G_{12} and G_{13} are listed in appendix A. For each wavevector and harmonic (each m , n , and j in Eq. (3.3)), the three boundary conditions are sufficient to determine the three unknowns α_{mn} , β_{mn} and δ_{mn} in (3.3). Because the algebra is quite involved (the number of terms is on the order of several thousand), we have in practice used a symbolic manipulation package to solve for these constants.

At order $\epsilon^{3/2}$ the equation of motion becomes,

$$(\partial_t \nabla^2 - \nu \nabla^2 \nabla^2) w_2 = -\partial_T \nabla^2 w_0 + \{\nabla \times \nabla \times [(\mathbf{u}_0 \cdot \nabla) \mathbf{u}_1 + (\mathbf{u}_1 \cdot \nabla) \mathbf{u}_0]\} \cdot \hat{\mathbf{e}}_z \quad (3.4)$$

At this order we only need to consider resonant terms; for example, all terms proportional to $\cos(\mathbf{k}_1 \cdot \mathbf{x})$. The right hand side of Eq.(3.4) is of the form,

$$\cos(\mathbf{k}_1 \cdot \mathbf{x}) \sum_{j=1,3,5,\dots} e^{ji\omega t/2} E_j(z). \quad (3.5)$$

where we have used the solutions $(\mathbf{u}_0, \zeta_0, \mathbf{u}_1, \zeta_1)$ already determined. Again, the $E_j(z)$ are combinations of exponential functions. The solutions for w_2 and ζ_2 are

$$w_2 = \cos(\mathbf{k}_1 \cdot \mathbf{x}) \sum_{j=1,3,5,\dots} e^{ji\omega t/2} [\bar{E}_j(z) + (a_j e^{kz} + b_j e^{q_j z}) C_j]$$

$$\zeta_2 = \cos(\mathbf{k}_1 \cdot \mathbf{x}) \sum_{j=1,3,5,\dots} e^{ji\omega t/2} C_j$$

Here $\bar{E}_j(z)$ is the particular solution that corresponds to the right hand side at this order shown in Eq.(3.5), and $a_j e^{kz} + b_j e^{q_j z}$ is the homogeneous solution, which has the same form as the linear solution. We now use the kinematic and tangential stress boundary conditions at this order to determine the constants a_j and b_j , so that the normal stress boundary condition yields a solvability condition for the amplitudes C_j , which in turn leads to the amplitude equations for the B_m . (Note that there are various terms of B_m in $\bar{E}_j(z)$.)

The boundary conditions at this order are

$$\begin{aligned} \partial_t \zeta_2 - w_2 &= G_{21}(\mathbf{u}_0, \zeta_0, \mathbf{u}_1, \zeta_1) \\ (\nabla_H^2 - \partial_{zz}) w_2 &= G_{22}(\mathbf{u}_0, \zeta_0, \mathbf{u}_1, \zeta_1) \\ (-\partial_t + 3\nu \nabla_H^2 + \nu \partial_{zz}) \partial_z w_2 + (g - \frac{\sigma}{\rho} \nabla_H^2 + f_0 \cos \omega t) \nabla_H^2 \zeta_2 &= G_{23}(\mathbf{u}_0, \zeta_0, \mathbf{u}_1, \zeta_1), \end{aligned}$$

where the functions G_{21} , G_{22} and G_{23} are listed in appendix A. By using the first two equations, a_j and b_j are found to be (again with the help of a symbolic manipulation package)

$$a_j C_j = \nu(k^2 + q_j^2) C_j + E_j^a$$

$$b_j C_j = -2\nu k^2 C_j + E_j^b.$$

Here E_j^a and E_j^b are complicated expressions involving the amplitudes of the waves, B_m . Now w_2 and ζ_2 are substituted into the third boundary equation to yield

$$\begin{aligned} H_1 C_1 - f_0 C_1^* - f_0 C_3 &= F_1, \\ H_3 C_3 - f_0 C_1 - f_0 C_5 &= F_3, \\ H_5 C_5 - f_0 C_3 - f_0 C_7 &= F_5, \quad \dots \end{aligned}$$

The left hand side of this system of equations is identical to Eq. (2.9) for the linear problem, and the functions F_j on the right hand side are functions of B_m and dB_1/dT .

Solving for C_j just like we solved for the linear threshold, we obtain

$$\bar{H}_1 C_1 - f_0 C_1^* = F_1 + \frac{f_0}{\bar{H}_3} \left(F_3 + \frac{f_0}{\bar{H}_5} (F_5 + \dots) \right) \equiv F,$$

with \bar{H}_j defined similarly to \bar{H}_1 in Eq. (2.11). Since the threshold of linear instability given by $f_0 = |\bar{H}_1|$, a nontrivial solution for C_1 will exist if the following solvability condition is satisfied:

$$F \bar{H}_1^* + F^* f_0 = 0.$$

This condition immediately leads to a standing wave amplitude equation for B_1 ,

$$\frac{dB_1}{dT} = \alpha B_1 - g_0 B_1^3 - \sum_{m \neq 1} g(\theta_{m1}) B_m^2 B_1, \quad (3.6)$$

with θ_{m1} the angle between \mathbf{k}_m and \mathbf{k}_1 . The linear coefficient α (times ϵ) is the linear growth or decay rate of this wave, and can be obtained from the linear analysis (simply consider an extra factor $e^{\alpha t}$ in Eq. (2.6)). The coefficient $g(\theta)$ describes the nonlinear interaction between different linearly unstable modes, and provides for the saturation of the wave amplitude. Figures 3 and 4 show our results for different values of γ and for $\Sigma = 0$ (pure gravity waves), and $\Sigma = 1/3$ (mixed gravity-capillary waves). It is also important to note the asymptotic behavior of $g(\theta)$ as $\nu \rightarrow 0$. We have already discussed in Sec. 2, that the irrotational component of the flow contributes to order ν to the linearized equation of motion (Eq. (2.8)), whereas the rotational flow contribution scales as $\nu^{3/2}$ instead. This observation is the basis for earlier low viscosity approximations in which only viscous dissipation arising from the irrotational flow was considered (Miles (1984), Milner (1991), Miles (1993)). However, we have computed the coefficient $g(\theta)$ with and without the linear rotational flow and observed that both contributions are of order ν at small ν . Therefore, a formulation that does not incorporate the rotational flow explicitly cannot obtain the correct form of the third order damping coefficients, even in the limit of small viscosity.

Particular nonlinear interaction terms that contribute to $g(\theta)$ are shown in Fig. 5. Two linearly unstable modes with wave vectors \mathbf{k}_m and \mathbf{k}_n ($|\mathbf{k}_m| = |\mathbf{k}_n| = k_{\text{onset}}$) interact to produce a wave at $\mathbf{k}_m + \mathbf{k}_n$ with an amplitude proportional to $B_m B_n$. This mode corresponds to a first order solution (w_1 and ζ_1 in Eqs. (3.2) and Eq. (3.3)). Now $\mathbf{k}_m + \mathbf{k}_n$ couples back to the original wave at $-\mathbf{k}_n$ to give a contribution $B_n^2 B_m$ to dB_m/dT . Since the mode $\mathbf{k}_m + \mathbf{k}_n$ is damped (only waves with wavenumbers near k_{onset} are unstable), this is a dissipative term and contributes to nonlinear saturation of the wave. Triad resonance occurs when the frequency of the mode $\mathbf{k}_m + \mathbf{k}_n$ equals the driving frequency (the modes \mathbf{k}_m and \mathbf{k}_n oscillate at half the driving frequency). Energy is now directly transferred into this mode which can have a very large amplitude at low damping. Since $\mathbf{k}_m + \mathbf{k}_n$ couples back to $-\mathbf{k}_n$, it provides a dissipation channel for the mode \mathbf{k}_n . Dissipation is enhanced by triad resonance and results in a large value of $g(\theta_{mn})$ in the vicinity of the resonant angle. The resonant angle can be estimated from the inviscid dispersion relation (2.13), written in dimensionless form,

$$\bar{\omega}^2 = G \bar{k} + \Sigma \bar{k}^3, \quad (3.7)$$

with $\bar{k} = 1$, and $\bar{\omega}^2 = G + \Sigma = 1$ for the linearly unstable mode. At resonance, we have $\bar{\omega} = 2$, and the resonant wave number $\bar{k}_r = |\mathbf{k}_m + \mathbf{k}_n|$ satisfies $\bar{k}_r (G + \Sigma \bar{k}_r^2) = 4$. If θ_r is the resonant angle between \mathbf{k}_m and \mathbf{k}_n , $\bar{k}_r = \sqrt{2(1 + \cos \theta_r)}$, the resonance condition

becomes

$$\sqrt{2(1 + \cos \theta_r)}[G + 2(1 + \cos \theta_r)\Sigma] = 4. \quad (3.8)$$

Because $G + \Sigma = 1$, this condition can only be satisfied when $\Sigma > 1/3$. For example, $\cos \theta_r = 2^{1/3} - 1$ for $\Sigma = 1$.

For finite damping, the resonance condition is modified. However, triad resonance is expected to be significant only at low damping because of the damped nature of the first order wave. For example, Fig. 6 shows $g(\theta)$ for different γ and $\Sigma = 1$. At small γ , the nonlinear coefficient grows near resonance and peaks at the resonant angle. The value of the peak is seen to decrease with increasing γ . At $\gamma = 0.1$, resonance has almost disappeared.

In the formulation presented earlier, resonance arises from the homogeneous solutions w_{1h} and ζ_1 , which require finding the constants α_{mn}, β_{mn} and δ_{mn} in Eq. (3.3) by enforcing the boundary conditions at first order. The boundary conditions give rise to a system of linear equations for α_{mn}, β_{mn} and δ_{mn} , the left hand side of which (its matrix form is explicitly given in appendix B) at $\gamma = 0$ has a determinant

$$8\bar{k}^2 (G\bar{k}^2 + \Sigma\bar{k}^4) [4\bar{k} - (G\bar{k}^2 + \Sigma\bar{k}^4)]^2,$$

which, when equated to zero, is equivalent to Eq. (3.8).

4. Pattern selection and comparison with experiments

Since the standing wave amplitude equation (3.6) can be written in gradient form, the selected pattern near threshold immediately follows (Cross & Hohenberg (1993)). Equation (3.6) is equivalent to

$$\frac{dB_n}{dT} = -\frac{\delta\mathcal{F}}{\delta B_n},$$

with the Lyapunov function \mathcal{F} given by

$$\mathcal{F} = -\frac{1}{2}\alpha \sum_m B_m^2 + \frac{1}{4} \sum_m \sum_n g(\theta_{mn}) B_m^2 B_n^2,$$

with $g_0 = g(\theta_{nn})$ which equals half the value of $g(\theta \rightarrow 0)$. The amplitude equation then implies that

$$\frac{d\mathcal{F}}{dT} = \sum_n \frac{\delta\mathcal{F}}{\delta B_n} \frac{dB_n}{dT} = -\sum_n \left(\frac{dB_n}{dT} \right)^2 \leq 0,$$

so that the preferred pattern can be determined by minimization of \mathcal{F} . The experimentally observed regular patterns above onset consist of N standing waves, with uniform amplitudes and wavevectors $\mathbf{k}_m, m = 1 \dots N$. The case $N = 1$ corresponds to a single standing wave (a pattern of parallel stripes), $N = 2$ to a pattern of square symmetry, $N = 3$ of hexagonal symmetry, etc. For these regular patterns, the standing wave amplitudes are

$$B_n^2 = \frac{\alpha}{g_0 + \sum_{m \neq n} g(\theta_{mn})}, \quad n = 1 \dots N.$$

The value of the Lyapunov function as a function of N then becomes

$$\mathcal{F}(N) = -\frac{\alpha^2}{4} \frac{N}{g_0 + \sum_{m=2}^N g(\theta_{m1})}. \quad (4.1)$$

Figure 7 shows the computed values of $\mathcal{F}(N)$ as a function of γ for different values of

Σ . For pure gravity waves ($\Sigma = 0$), the $N = 1$ state has the lowest value of the Lyapunov function and hence will be the selected pattern. At low frequency, the system effectively crosses over to the large damping region regardless of its (finite) viscosity (this range was not accessible to the low damping calculation of Zhang & Viñals (1997)). On the other hand, for pure capillary waves ($\Sigma = 1$) the preferred pattern is $N = 2$ at low damping and $N = 1$ at high damping. Interesting behavior is observed in the vicinity of $\Sigma = 1/3$ (mixed gravity capillary waves) where the triad resonance angle approaches zero. Hexagonal and higher symmetry quasipatterns are selected with decreasing γ . The low damping results in this region are in qualitative agreement with the earlier work of Zhang & Viñals (1997), although the latter could not account for the transition to $N = 1$ as γ is increased.

We finally compare our predictions (based on Eq. (4.1)) and two recent sets of experiments that addressed pattern selection in the large aspect ratio limit by Kudrolli & Gollub (1996) and by Binks & van de Water (1997). The only input parameters in our calculations are the fluid properties (density, surface tension and viscosity), and the frequency of the driving acceleration. All these parameters are known fairly precisely in the experimental work, thus allowing a quantitative comparison between theory and experiments.

Pattern selection in the low viscosity range has been recently studied by Binks & van de Water (1997). They have developed a cell of exceptionally large aspect ratio, and of depth that is much larger than the wavelength. The fluid used was a low viscosity, low surface tension silicon oil with $\nu = 0.03397 \text{ cm}^2/\text{s}$, $\rho = 0.8924 \text{ g/cm}^3$ and $\sigma = 18.3 \text{ dyne/cm}$. Given the range of frequencies studied, the viscous damping parameter probed was within $\gamma \sim 0.01 - 0.03$. They have reported transitions from standing wave patterns of square symmetry at high frequency ($\approx 41 \text{ Hz}$), to hexagonal, eight-fold and ten-fold quasi-periodic patterns upon lowering the driving frequency. Stable hexagonal patterns appear at approximately 36 Hz, although a transition region of mixed square/hexagonal symmetry is observed between approximately 36 Hz and 41 Hz. Given the parameters of this experiment, our theory predicts a transition at 35.4 Hz, compared to the value of 32.8 Hz given by the earlier work of Zhang & Viñals (1997). An additional transition region exhibiting patterns of mixed hexagonal and eight-fold symmetry was also observed between 30-31 Hz, which compares favorably with our prediction for the transition to eight-fold symmetric patterns at 28.7 Hz (Zhang & Viñals (1997) had predicted the transition to occur at 27.9 Hz). † A possible explanation for the larger discrepancy between the experiments and the calculations of Zhang & Viñals (1997) involves the fact that they only used the term linear in γ in the calculation of the threshold for instability (Eq. (2.14)). Omitting the first correction (of order $\gamma^{3/2}$) yields a similar percentage error in the threshold value (for γ in the range 0.01 - 0.03 as is appropriate for this experiment).

Another set of recent experiments involving fluids of different viscosity has been carried out by Kudrolli & Gollub (1996). Although the depth of the fluid layer (0.3 cm) is smaller than the wavelength of the waves (1-3 cm), the comparison is still illuminating. Figure 8 shows the symmetry of the predicted patterns as a function of the viscosity of the fluid and of the driving frequency (with $\rho = 0.95 \text{ g/cm}^3$ and $\sigma = 20.6 \text{ dyn/cm}$), and the experimentally observed patterns. They find a stripe pattern at high viscosity, a hexagonal pattern at low viscosity and frequency, and a square pattern at low viscosity and high frequency. Two significant discrepancies concern the experimental observation of a hexagonal pattern at $\nu = 1 \text{ cm}^2/\text{s}$ and low frequency, and also at $\nu = 0.04 \text{ cm}^2/\text{s}$

† In this experiment, patterns with $N = 5$ are observed around 27 Hz. We agree with the authors of the experiment that this discrepancy may be due to finite size effects. In fact, $\mathcal{F}(5)$ is very close to $\mathcal{F}(4)$ at about 26 Hz (the difference is less than 0.2%), although $\mathcal{F}(5) > \mathcal{F}(4)$.

and $f = 27\text{Hz}$. It is possible that the shallowness of the fluid layer can account for these differences, especially in view of the fact that, as noted above, the experiments by Binks & van de Water (1997) did probe this latter region in a deep fluid layer, and their results do agree with our predictions.

Finally, the fact that portions of the boundaries separating regions of different symmetry appear almost as straight lines in Fig. 8 is due to the log-log scale used. In addition, the transition line delimiting the region of stripe patterns is almost independent of frequency only because of the limited frequency range probed in the experiments and displayed in the figure. On the other hand, the line separating regions of square and hexagonal patterns is almost independent of viscosity because it depends mainly on whether the waves are capillarity or gravity dominated, fact that is largely dependent on the driving frequency and not on viscosity.

In summary, we have presented a nonlinear theory for Faraday waves in viscous fluids with no assumptions or approximations other than those inherent to the multi-scale expansion. A set of standing wave amplitude equations has been obtained that is of gradient form. Minimization of the associated Lyapunov function leads to determination of the preferred pattern near threshold. The predicted patterns are in excellent agreement with recent experiments in large aspect ratio systems involving a range of fluid viscosities and driving frequencies. According to Fig. 7, the transition from square to stripe patterns remains in the capillary wave limit of $\Sigma = 1$ (high frequency limit in the experiments). However, the figure for $\Sigma = 0$ indicates that stripe patterns are always preferred in the pure-gravity-wave limit (low frequency limit in the experiments). Furthermore, all the high symmetry patterns (with $N \geq 3$) are observed in the vicinity of $\Sigma = 1/3$, point at which the triad resonant angle approaches zero, and for low damping where the resonance is more pronounced.

This research has been supported by the U.S. Department of Energy, contract No. DE-FG05-95ER14566, and also in part by the Supercomputer Computations Research Institute, which is partially funded by the U.S. Department of Energy, contract No. DE-FC05-85ER25000.

Appendix A. Inhomogeneous terms of the first and second order equations

We list in this appendix the functions G_{ij} , the inhomogeneous terms in the boundary conditions at first and second order.

$$\begin{aligned}
G_{11} &= \partial_z w_0 \zeta_0 - u_0 \partial_x \zeta_0 - v_0 \partial_y \zeta_0, \\
G_{12} &= \partial_x [-\partial_{zz} u_0 \zeta_0 - \partial_{xz} w_0 \zeta_0 + 2(\partial_x u_0 - \partial_z w_0) \partial_x \zeta_0 + (\partial_y u_0 + \partial_x v_0) \partial_y \zeta_0] \\
&\quad + \partial_y [-\partial_{zz} v_0 \zeta_0 - \partial_{yz} w_0 \zeta_0 + 2(\partial_y v_0 - \partial_z w_0) \partial_y \zeta_0 + (\partial_x v_0 + \partial_y u_0) \partial_x \zeta_0], \\
G_{13} &= -\rho \nabla_H \cdot [(\mathbf{u}_0 \cdot \nabla) \mathbf{u}_0] + \nabla_H^2 (-2\eta \partial_{zz} w_0 \zeta_0 + \partial_z p_0 \zeta_0) \\
G_{21} &= -\partial_T \zeta_0 - u_0 \partial_x \zeta_1 - u_1 \partial_x \zeta_0 - \partial_z u_0 \zeta_0 \partial_x \zeta_0 - v_0 \partial_y \zeta_1 - v_1 \partial_y \zeta_0 - \partial_z v_0 \zeta_0 \partial_y \zeta_0 \\
&\quad + \partial_z w_0 \zeta_1 + \partial_z w_1 \zeta_0 + \frac{1}{2} \partial_{zz} w_0 \zeta_0^2, \\
G_{22} &= \partial_x \left[-\partial_{zz} u_1 \zeta_0 - \partial_{zz} u_0 \zeta_1 - \frac{1}{2} \partial_{zzz} u_0 \zeta_0^2 - \partial_{xz} w_1 \zeta_0 - \partial_{xz} w_0 \zeta_1 - \frac{1}{2} \partial_{xzz} w_0 \zeta_0^2 \right. \\
&\quad \left. - 2(\partial_z w_1 - \partial_x u_1) \partial_x \zeta_0 - 2(\partial_z w_0 - \partial_x u_0) \partial_x \zeta_1 - 2\partial_z (\partial_z w_0 - \partial_x u_0) \zeta_0 \partial_x \zeta_0 \right. \\
&\quad \left. + (\partial_y u_1 + \partial_x v_1) \partial_y \zeta_0 + (\partial_y u_0 + \partial_x v_0) \partial_y \zeta_1 + \partial_z (\partial_y u_0 + \partial_x v_0) \zeta_0 \partial_y \zeta_0 \right] \\
&\quad + \partial_y \left[-\partial_{zz} v_1 \zeta_0 - \partial_{zz} v_0 \zeta_1 - \frac{1}{2} \partial_{zzz} v_0 \zeta_0^2 - \partial_{yz} w_1 \zeta_0 - \partial_{yz} w_0 \zeta_1 - \frac{1}{2} \partial_{yzz} w_0 \zeta_0^2 \right. \\
&\quad \left. - 2(\partial_z w_1 - \partial_y v_1) \partial_y \zeta_0 - 2(\partial_z w_0 - \partial_y v_0) \partial_y \zeta_1 - 2\partial_z (\partial_z w_0 - \partial_y v_0) \zeta_0 \partial_y \zeta_0 \right. \\
&\quad \left. + (\partial_y u_1 + \partial_x v_1) \partial_x \zeta_0 + (\partial_y u_0 + \partial_x v_0) \partial_x \zeta_1 + \partial_z (\partial_y u_0 + \partial_x v_0) \zeta_0 \partial_x \zeta_0 \right] \\
G_{23} &= -\rho \nabla_H \cdot [(\mathbf{u}_0 \cdot \nabla) \mathbf{u}_1 + (\mathbf{u}_1 \cdot \nabla) \mathbf{u}_0] + \rho \partial_T \partial_z w_0 + \nabla_H^2 \left[-\frac{1}{2} \rho f_0 (e^{i\omega t} + e^{-i\omega t}) \zeta_0 \right. \\
&\quad \left. + \partial_z p_1 \zeta_0 + \partial_z p_0 \zeta_1 + \frac{1}{2} \partial_z^2 p_0 \zeta_0^2 - 2\eta \partial_z^2 w_1 \zeta_0 - 2\eta \partial_z^2 w_0 \zeta_1 - \eta \partial_z^3 w_0 \zeta_0^2 \right. \\
&\quad \left. + 2\eta (\partial_z u_1 + \partial_x w_1) \partial_x \zeta_0 + 2\eta (\partial_z w_0 - \partial_x u_0) (\partial_x \zeta_0)^2 \right. \\
&\quad \left. + 2\eta (\partial_z v_1 + \partial_y w_1) \partial_y \zeta_0 + 2\eta (\partial_z w_0 - \partial_y v_0) (\partial_y \zeta_0)^2 \right. \\
&\quad \left. - 2\eta (\partial_y u_0 + \partial_x v_0) \partial_x \zeta_0 \partial_y \zeta_0 - \frac{3}{2} \sigma \partial_{xx} \zeta_0 (\partial_x \zeta_0)^2 - \frac{3}{2} \sigma \partial_{yy} \zeta_0 (\partial_y \zeta_0)^2 \right. \\
&\quad \left. - \frac{1}{2} \sigma \partial_{xx} \zeta_0 (\partial_y \zeta_0)^2 - \frac{1}{2} \sigma \partial_{yy} \zeta_0 (\partial_x \zeta_0)^2 - 2\sigma \partial_x \zeta_0 \partial_y \zeta_0 \partial_{xy} \zeta_0 \right].
\end{aligned}$$

Appendix B. Matrix of coefficients at first order

Left hand side of the system of linear equations for the first order solution (for simplicity, we only show the case $\gamma \ll 1$ and the coefficients of first time harmonic $e^{i\omega t/2}$),

$$\begin{pmatrix} -1 & 0 & 0 & -1 & 0 & 0 & -2i & 0 & 0 \\ 0 & -1 & 0 & 0 & -1 & 0 & 0 & 0 & 0 \\ 0 & 0 & -1 & 0 & 0 & -1 & 0 & 0 & 2i \\ -\gamma\bar{k}^2 & 0 & 0 & 2i & 0 & 0 & 0 & 0 & 0 \\ 0 & -\bar{k}^2 & 0 & 0 & -\bar{k}^2 & 0 & 0 & 0 & 0 \\ 0 & 0 & -\gamma\bar{k}^2 & 0 & 0 & -2i & 0 & 0 & 0 \\ -2i\bar{k} & 0 & 0 & \gamma\bar{k}^2\bar{q}^* & 0 & 0 & G\bar{k}^2 + \Sigma\bar{k}^4 & 2\gamma\bar{k}^2 & 0 \\ 0 & \gamma\bar{k}^3 & 0 & 0 & 0 & 0 & 2\gamma\bar{k}^2 & G\bar{k}^2 + \Sigma\bar{k}^4 & 2\gamma\bar{k}^2 \\ 0 & 0 & 2i\bar{k} & 0 & 0 & \gamma\bar{k}^2\bar{q} & 0 & 2\gamma\bar{k}^2 & G\bar{k}^2 + \Sigma\bar{k}^4 \end{pmatrix} \begin{pmatrix} \alpha_{mn}^{1-} \\ \alpha_{mn}^0 \\ \alpha_{mn}^{1+} \\ \beta_{mn}^{1-} \\ \beta_{mn}^0 \\ \beta_{mn}^{1+} \\ \delta_{mn}^{1-} \\ \delta_{mn}^0 \\ \delta_{mn}^{1+} \end{pmatrix}$$

with $\bar{k} = |\bar{\mathbf{k}}_m + \bar{\mathbf{k}}_n|$ and $\bar{q}^2 \equiv \bar{k}^2 + 2i/\gamma$.

REFERENCES

- BENJAMIN, T.B. & URSELL, F. 1954 *Proc. R. Soc. Lond. A* **225**, 505.
- BESSON, T & EDWARDS, W.S. 1996 *Phys. Rev. E* **54** 507.
- BINKS, D. & VAN DE WATER, W. 1997 *Phys. Rev. Lett.* **78** 4043.
- CHRISTIANSEN, B, ALSTRØM, P. & LEVINSSEN, M.T. 1992 *Phys. Rev. Lett.* **68**, 2157.
- CILIBERTO, S., DOUADY, S. & FAUVE, S. 1991 *Europhys. Lett.* **15**, 23.
- COULLET, P., FRISCH, T. & SONNINO, G. 1994 *Phys. Rev. E* **49**, 2087.
- CROSS, M.C. & HOHENBERG, P.C. 1993 *Rev. Mod. Phys.* **65**, 851.
- DAUDET, L., EGO, V., MANNEVILLE, S. & BECHHOEFER, J. 1995 *Europhys. Lett.* **32**, 313.
- EDWARDS, W.S. & FAUVE, S. 1993 *Phys. Rev. E* **47**, R788.
- EDWARDS, W.S. & FAUVE, S. 1994 *J. Fluid Mech.* **278**, 123.
- EZERSKII, A.B., RABINOVICH, M.I., REUTOV, V.P. & STAROBINETS, I.M. 1986 *Zh. Eksp. Teor. Fiz.* **91** 1986 [*Sov. Phys. JETP* **64**, 1228].
- FARADAY, M. 1831 *Phil. Trans. R. Soc. Lond.* **121**, 319.
- HANSEN, P. L. & ALSTRØM, P. 1997 *preprint*.
- KUDROLLI, A. & GOLLUB, J.P. 1996 *Physica D* **97**, 133.
- KUMAR, K. & TUCKERMAN, L.S. 1994 *J. Fluid Mech.* **279**, 49.
- LAMB, H. 1995 *Hydrodynamics*, 6th Ed., Dover.
- LANDAU, L.D. & LIFSHITZ, E.M. 1959 *Fluid Mechanics*, Pergamon.
- LANDAU L.D. & LIFSHITZ, E.M. 1976 *Mechanics*, 3rd ed., Pergamon.
- LANG, R.J. 1962 *J. Acoust. Soc. Amer.* **34**, 6.
- LUNDGREN, T.S. & MANSOUR, N.N. 1988 *J. Fluid Mech.* **194**, 479.
- MILES, J.W. 1977 *J. Fluid Mech.* **83**, 153.
- MILES, J.W. 1984 *J. Fluid Mech.* **146**, 285.
- MILES, J.W. & HENDERSON, D. 1990 *Annu. Rev. Fluid Mech.* **22**, 143.
- MILES, J.W. 1993 *J. Fluid Mech.* **248**, 671; *ibid* 1994 **269**, 353.
- MILNER, S.T. 1991 *J. Fluid Mech.* **225**, 81.
- MÜLLER, H.W. 1993 *Phys. Rev. Lett.* **71**, 3287.
- MÜLLER, H.W. 1994 *Phys. Rev. E* **49**, 1273.
- MÜLLER, H.W. *et. al.* 1997 *Phys. Rev. Lett.* **78**, 2357.
- NAM HONG, U. 1993 *Bulletin of the Russian Academy of Sciences - Physics/Supplement* **57**, 131.
- NEWELL, A.C. & WHITEHEAD, J.A. 1969 *J. Fluid Mech.* **38**, 279.
- TORRES, M., PASTOR, I., JIMÉNEZ, I. & MONTERO DE ESPINOSA, F. 1995 *Chaos, Solitons & Fractals* **5**, 2089.
- TUFILLARO, N.B, RAMSHANKAR, R. & GOLLUB, J.P. 1989 *Phys. Rev. Lett.* **62**, 422.
- ZAKHAROV, V.E. 1968 *Zh. Prikl. Mekh. Tekh. Fiz.* **9**, 86 [*J. Appl. Mech. Tech. Phys.* **9**, 190].
- ZHANG W. & VIÑALS, J. 1996 *Phys. Rev. E* **53**, R4286.
- ZHANG W. & VIÑALS, J. 1997 *J. Fluid Mech.* **336**, 301.

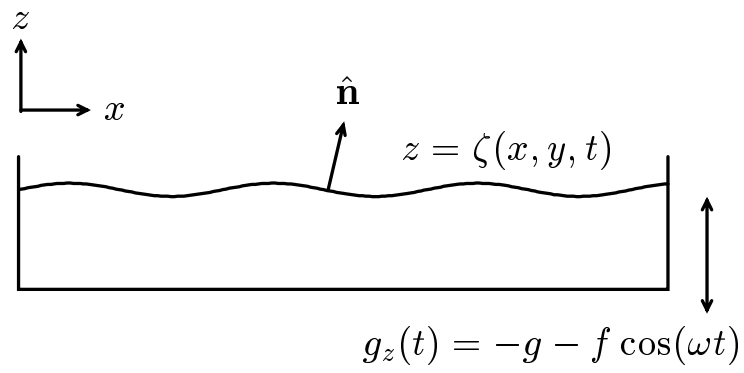


FIGURE 1. Schematic setup of a Faraday wave configuration.

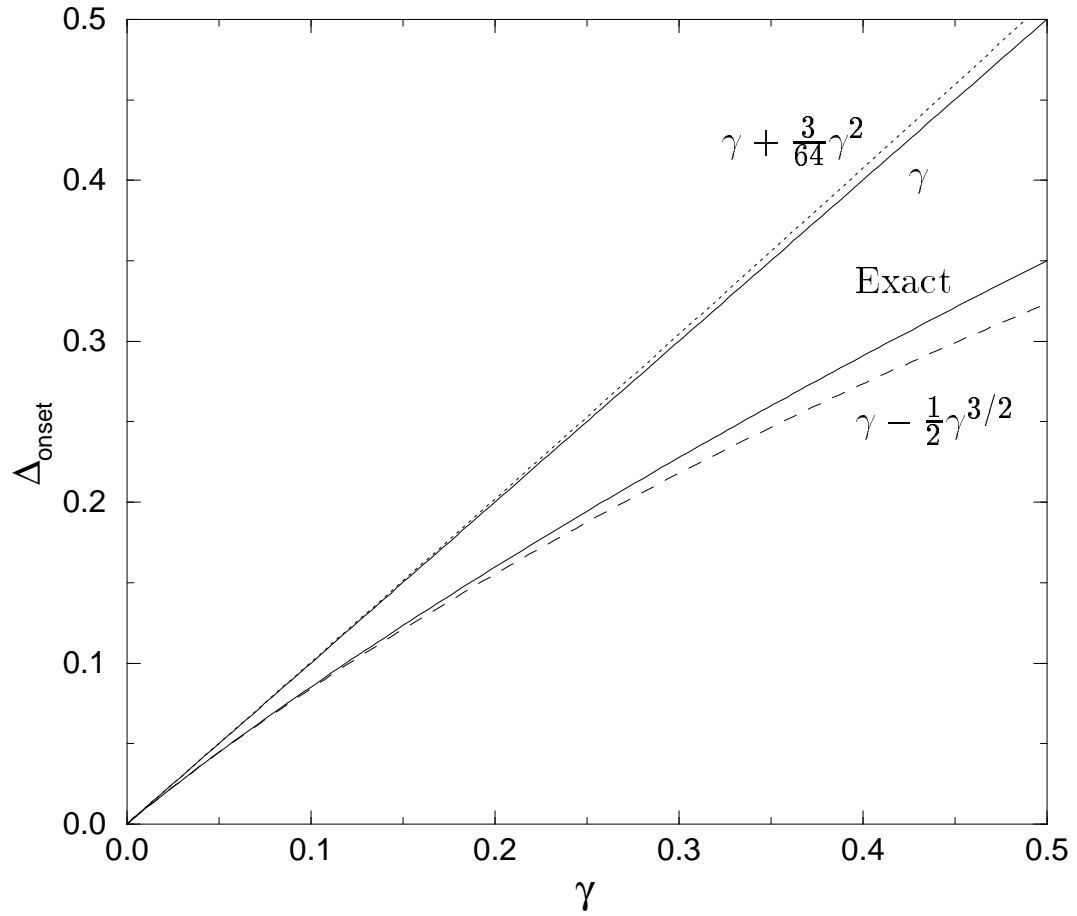


FIGURE 2. Dimensionless threshold for linear instability Δ_{onset} as a function of the dimensionless damping parameter γ . The lower solid line is the exact result; the upper solid line is the lowest order approximation in the damping parameter. Also shown are the first order correction in the viscous damping parameter (dashed line), and the first correction for the instability threshold for a damped Mathieu equation.

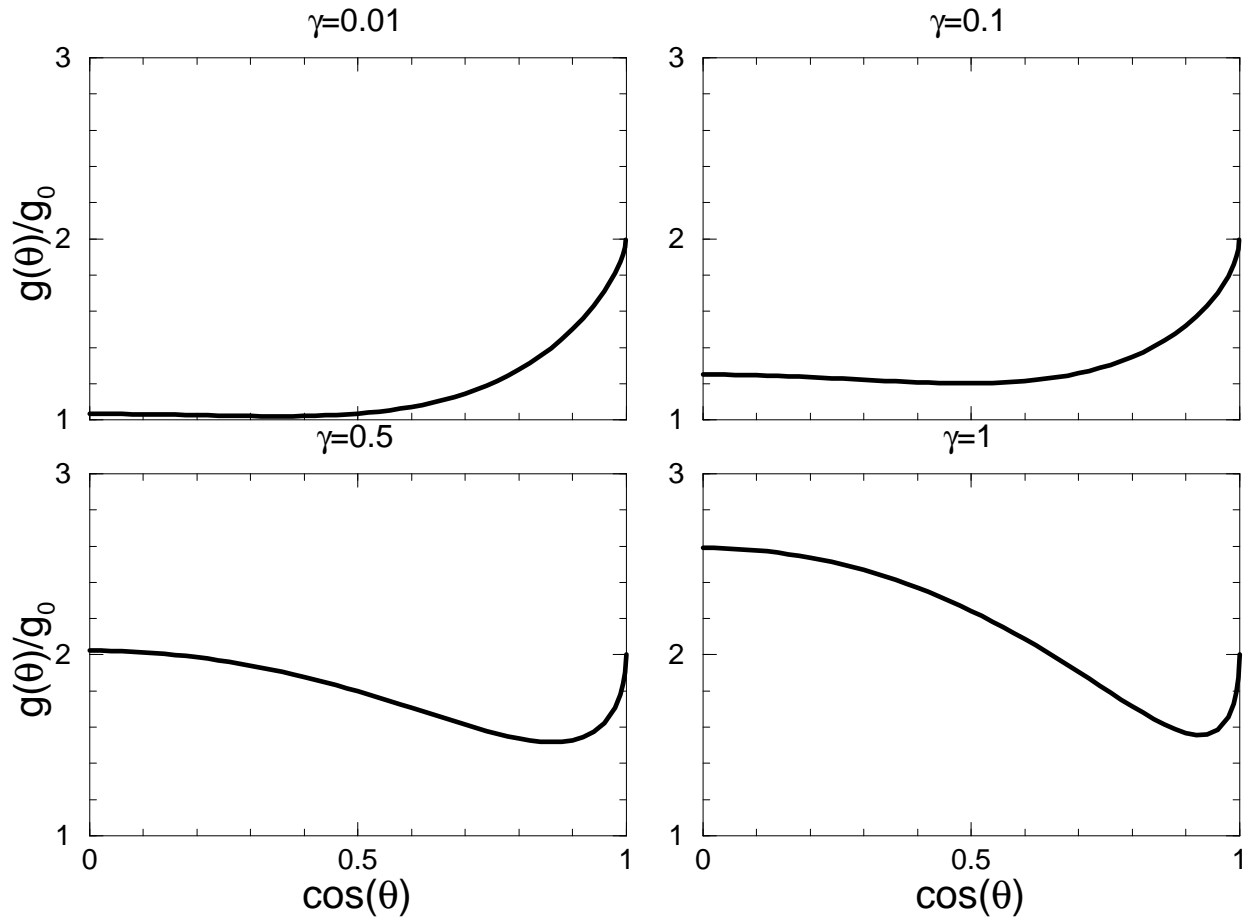


FIGURE 3. Cubic term coefficient of the standing wave amplitude equation as a function of angle between wavevectors θ , in the limit of gravity waves, $\Sigma = 0$, and different viscous damping coefficients.

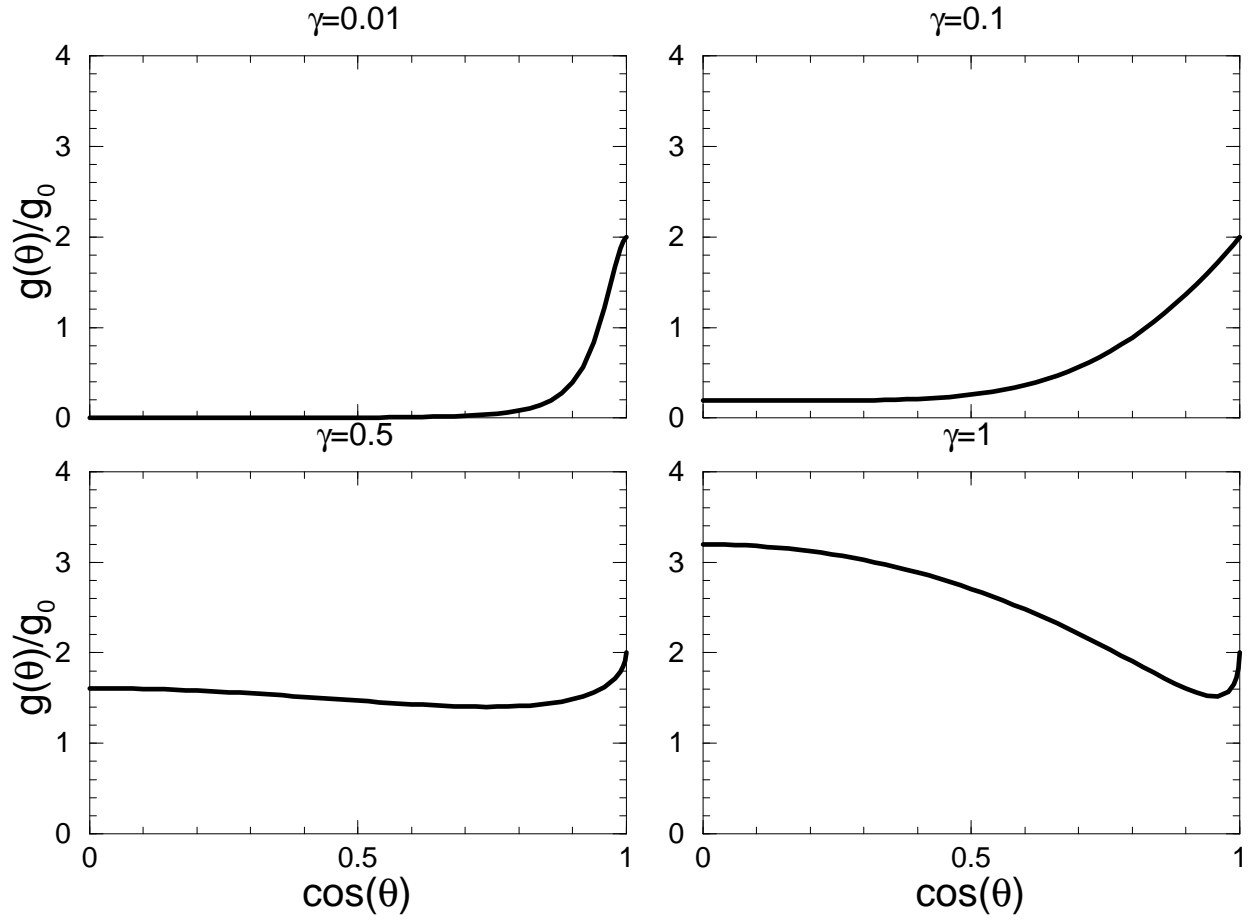


FIGURE 4. Cubic term coefficient of the standing wave amplitude equation as a function of angle between wavevectors θ , in the mixed capillary-gravity regime ($\Sigma = 1/3$). Note that the curve becomes extremely flat near $\cos \theta = 0$ for low γ .

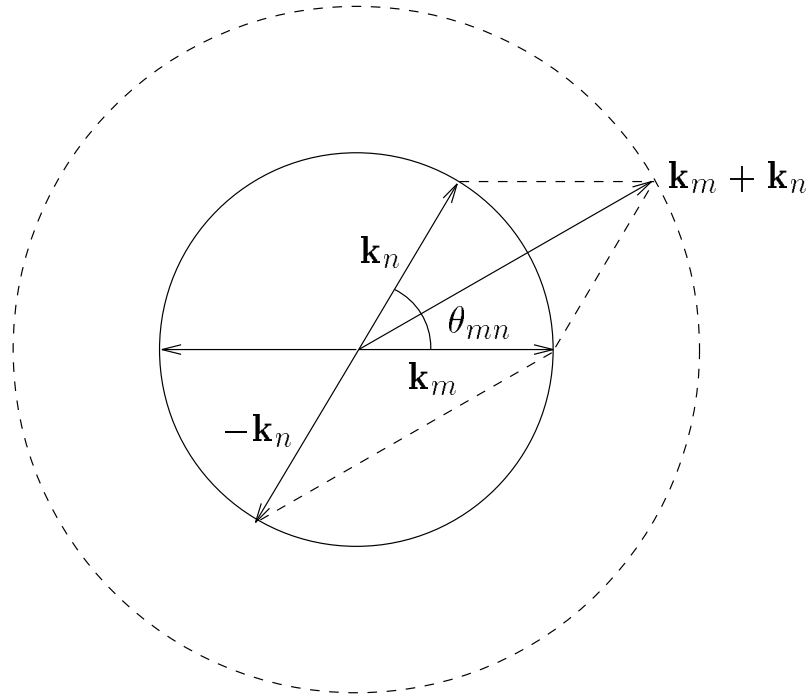


FIGURE 5. Schematic representation of a triad resonant interaction: two linearly unstable modes \mathbf{k}_m and \mathbf{k}_n interact to produce a linearly stable mode. This mode interacts with $-\mathbf{k}_n$ leading to resonance with \mathbf{k}_m .

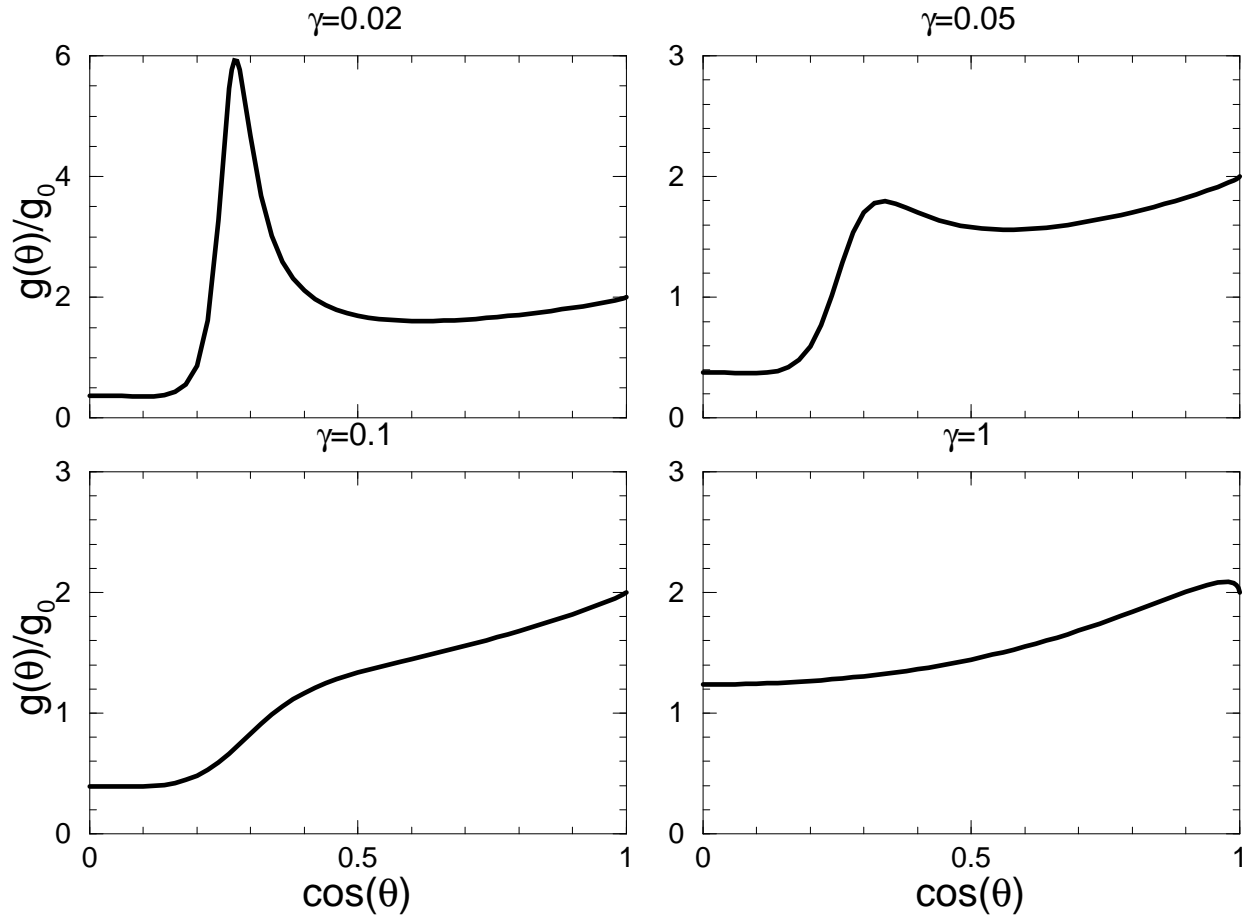


FIGURE 6. Cubic term coefficient of the standing wave amplitude equation as a function of angle between wavevectors θ , in the limit of capillary waves, $\Sigma = 1$. The large peaks at small values of γ are due to triad resonant interactions.

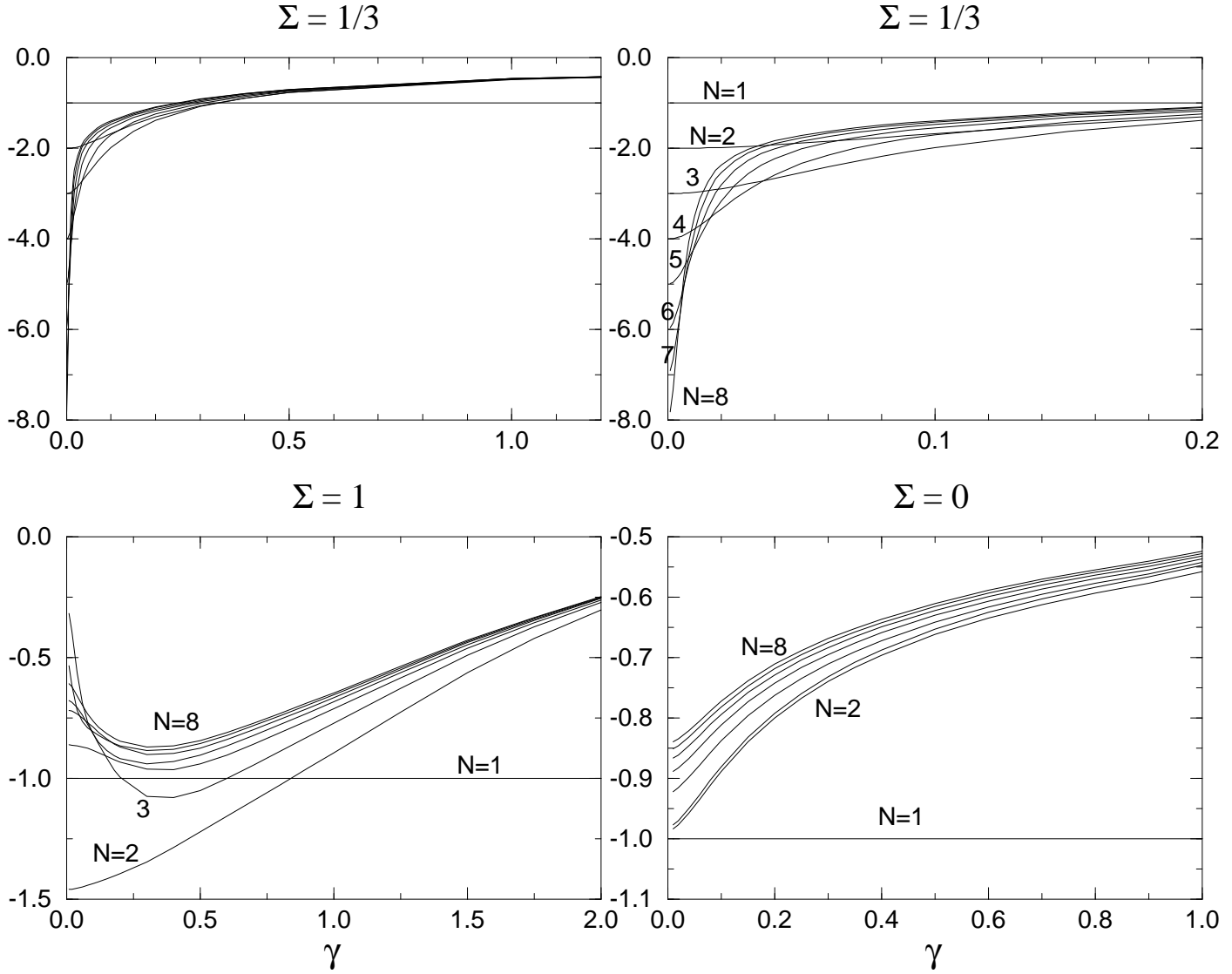


FIGURE 7. Numerical values of the Lyapunov function for regular patterns comprising N standing waves as a function of the viscous damping parameter γ . Bottom right: gravity wave limit; bottom left: capillary wave limit; top left, the mixed case of $\Sigma = 1/3$; top right is the same as top left but showing the region of small damping in more detail. In the two bottom plots, the curves not labeled are ordered in increasing order of N .

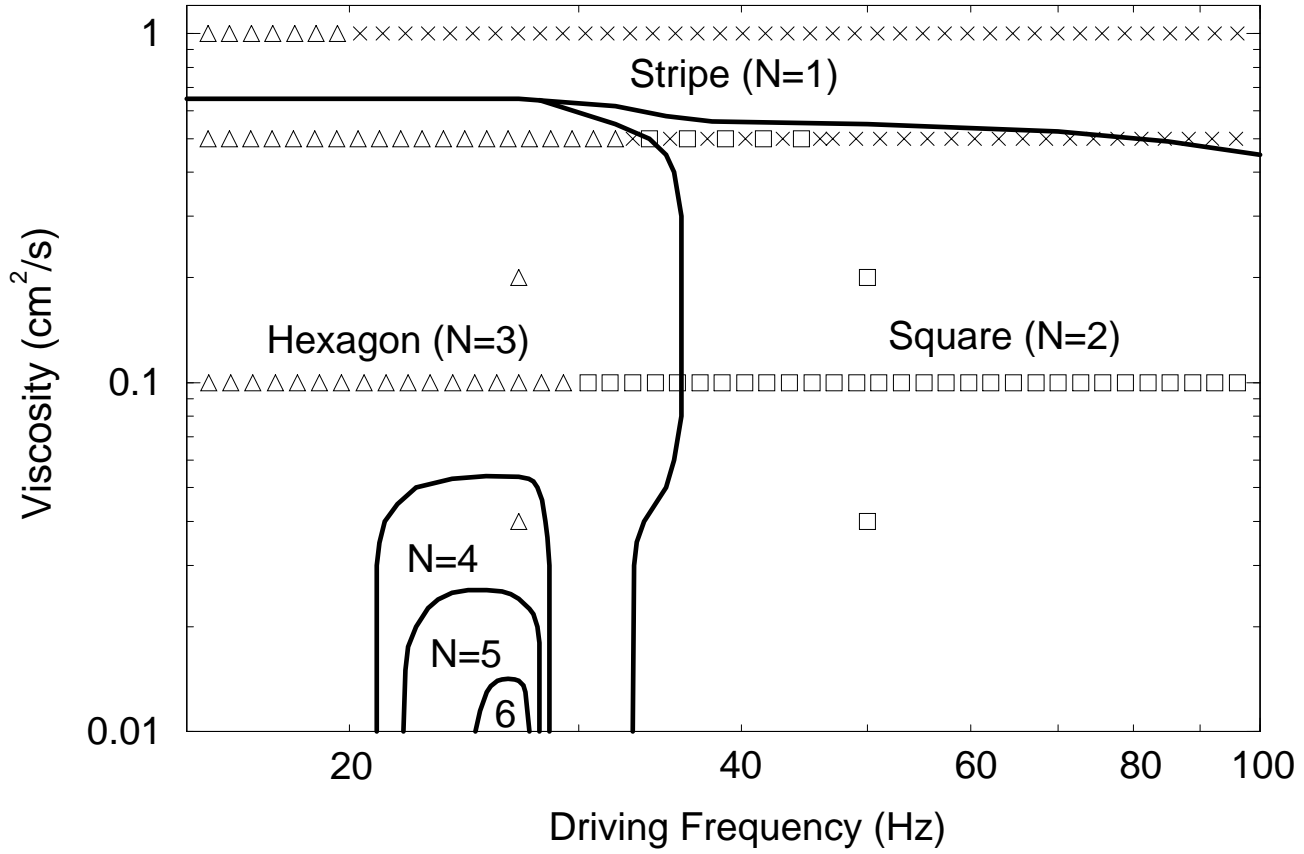


FIGURE 8. Selected patterns as a function of fluid viscosity and driving frequency. The symbols are the experimental results of Kudrolli & Gollub (1996). \times , stripe patterns; \square , square patterns; and, \triangle , hexagonal patterns. Alternating \times and \square indicate regions in which stationary mixed stripe and square patterns were observed.